Interpolated Average CT for Attenuation Correction in PET—A Simulation Study

Greta S. P. Mok, *Member, IEEE*, Tao Sun, *Student Member, IEEE*, Tzung-Chi Huang*, and Mang I. Vai, *Senior Member, IEEE*

***Abstract*—Previously, we proposed using an interpolated average CT (IACT) method for attenuation correction (AC) in positron emission tomography (PET), which is a good, low-dose approximation of cine average CT (CACT) to reduce misalignments and improve quantification in PET/CT. This study aims to evaluate the performance of IACT for different motion amplitudes. We used the digital four-dimensional (4-D) extended cardiac-torso phantom (XCAT) to simulate maximum of 2, 3, and 4 cm respiratory motions. The respiratory cycle was divided into 13 phases, with average activity and attenuation maps to represent ^{18}F-fluorodeoxyglucose (^{18}F-FDG) distributions with average respiratory motions and CACT, respectively. The end-inspiration, end-expiration, and midrespiratory phases of the XCAT attenuation maps represented three different helical CTs (i.e., HCT-1, HCT-5, and HCT-8). The IACTs were generated using: 1) 2 extreme + 11 interpolated phases ($IACT_{2o}$); 2) 2 phases right after the extreme phases + 11 interpolated phases ($IACT_{2s}$); 3) 4 original + 9 interpolated phases ($IACT_{4o}$). A spherical lesion with a target-to-background ratio (TBR) of 4:1 and a diameter of 25 mm was placed in the base of right lung. The noise-free and noisy sinograms with attenuation modeling were generated and reconstructed with different noise-free and noisy AC maps (CACT, HCTs, and IACTs) by Software for Tomographic Image Reconstruction, respectively, using ordered subset expectation maximization(OS-EM) with up to 300 updates. Normalized mean-square error, mutual information (MI), TBR, image profile, and noise-contrast tradeoff were analyzed. The PET reconstructed images with AC using CACT showed least difference as compared to the original phantom, followed by $IACT_{4o}$, $IACT_{2o}$, $IACT_{2s}$, HCT-5, HCT-8, and HCT-1. Significant artifacts were observed in the reconstructed images using HCTs for AC. The MI differences between $IACT_{2o}$ and $IACT_{4o}$/CACT were $<0.41\%$ and $<2.17\%$, respectively. With a slight misplacement of the two extreme phases, $IACT_{2s}$ was still comparable to $IACT_{2o}$ with MI difference of $<2.23\%$. The IACT is a robust and accurate low-dose alternate to CACT.**

***Index Terms*—Attenuation correction (AC), positron emission tomography (PET)/CT, respiratory artifacts, simulations.**

Manuscript received October 10, 2012; revised January 8, 2013; accepted January 28, 2013. Date of publication February 6, 2013; date of current version June 24, 2013. This work was supported in part by the University of Macau under Multiyear Research Grant MYRG185(Y2-L3)-FST11-MSP and Grant MYRG077(Y1-L2)-FST12-MSP. *Asterisk indicates corresponding author.*

G. S. P. Mok, T. Sun, and M. I. Vai are with the Department of Electrical and Computer Engineering, Faculty of Science and Technology, University of Macau, Macau, China (e-mail: gretamok@umac.mo; mb05470@umac.mo; fstmiv@umac.mo).

*T.-C. Huang is with the Department of Biomedical Imaging and Radiological Sciences, China Medical University, Taichung 40402, Taiwan (e-mail: tzungchi.huang@mail.cmu.edu.tw).

Color versions of one or more of the figures in this paper are available online at http://ieeexplore.ieee.org.

Digital Object Identifier 10.1109/TBME.2013.2245132

I. Introduction

RESPIRATORY motion is generally considered the main problem in the CT-based attenuation correction (AC) in positron emission tomography (PET)/CT. For conventional diagnostic CT, a three-dimensional (3-D) helical acquisition of the thoracic cavity is collected over a single full-inspiration breath-hold CT scan. When applied with the emission exam, the helical CT is usually applied during normal end-expiration breath-hold or shallow free breathing state [1]. This technique captures a snapshot of the thoracic cavity in a distinct respiratory phase and does not represent the time-averaged position of the thoracic structures as PET acquisition does. In fact, for thoracic structures, more than 40% studies have misalignments between the PET and CT data [2]. Erdi *et al.* [3] examined PET/CT images of five lung carcinoma patients with multiple lesions and showed that spatial mismatch resulted in up to a 30% error in the standardized uptake value (SUV) of the lesions. Also, phantom studies showed that the effect of motion could result in as much as 75% underestimation of the maximum activity concentrations [4]. These distortions may lead to inaccurate localization of tumors and hence potential misdiagnoses [5], [6].

Various techniques have been developed to mitigate the PET/CT misalignments and improve the quantitative accuracy, and gated four-dimensional (4-D) PET/CT is one of the growing research areas [7], [8]. Nehmeh *et al.* [9] spatially matched the 4-D CT data with the gated PET images according to the externally monitored breathing signal and showed improved lesion registration, with the cost of increasing CT radiation dose. McQuaid *et al.* [10] proposed aligning a single CT with each gated frame of PET via a statistical shape model of the diaphragm and a rigid registration of the heart to improve quantitative accuracy. Similar investigation was also proposed by Wells *et al.* [11]. Liu *et al.* [12] developed a quiescent period gating method to utilize the end-expiration quiescent phase of PET data to match with the end-expiration CT. Li *et al.* [13] and Qiao *et al.* [14] incorporated motion estimation into the iterative reconstruction process to lower image noise of a gated PET frame that had lower counts. Lamare *et al.* [15] integrated elastic motion correction into the system matrix in the PET reconstruction process. Grotus *et al.* [16] introduced the 4-D joint-estimation algorithm to form a new 4-D OS-EM reconstruction method for gated PET images.

Besides 4-D PET/CT, other CT protocol-based methods were also used to address the misalignment artifacts. Lagerwaard *et al.* [17] introduced slow CT and Nye *et al.* [18] suggested low-pitch CT for AC, with the same intention to lengthen the CT acquisition in order to capture the average respiratory position

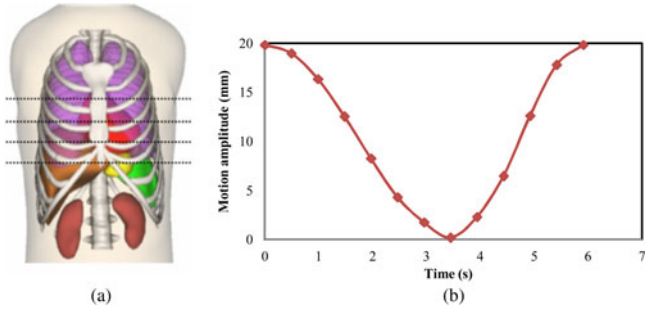

Fig. 1. (a) The XCAT phantom and (b) the respiratory cycle was divided into 13 phases (2 cm maximum diaphragm motion is shown here).

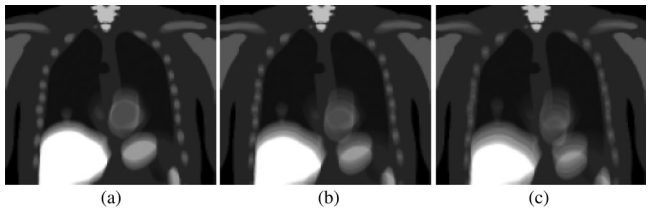

Fig. 2. The average noise-free activity maps showing (a) 2 cm, (b) 3 cm, and (c) 4 cm maximum respiratory motions.

of the thoracic cavity as in PET. Cine-average CT (CACT) from a 4-D CT acquisition for AC has been proposed to reduce the misalignment artifacts and improve quantification of PET/CT [14], [19], [20] as compared to the conventional helical CT (HCT), while Alessio *et al*. [21] suggested that the intensity-maximum cine image gave more impressive and robust results as compared to CACT. Efforts have been addressed to reduce the radiation exposure for CACT, such as lowering tube currents [22], [23] and modifying the acquisition protocol [24]. Sun and Mok [25] published a detailed review regarding different PET/CT respiratory artifacts reduction methods.

Previously, we have developed a new interpolated average CT (IACT) method, potentially generated from averaging the free-breathing end-expiration, end-inspiration, and interpolated phases obtained using deformable image registration, as a low-dose alternate to CACT for AC in PET/CT [26]. We have demonstrated its clinical merits on six oncologic patients and also potential applications in cardiology [27]. That was a patient study, and PET images using CACT for AC were used as the gold standard, while the "true" PET activity distributions were not available for comparison. This study aims to evaluate its accuracy and robustness, i.e., effects of different respiratory motion amplitudes and misplacement of the two extreme phases, based on computer simulations with known truth.

II. Materials and Methods

In this study, we simulated the sinograms with attenuation effects from the digital 4-D extended cardiac-torso (XCAT) phantom [see Fig. 1(a)] that realistically models the anatomy, activity distribution of a male patient injected with ^{18}F-FDG, and the respiratory motions. We used an analytical projector and OS-EM reconstruction algorithm provided by Software for Tomographic Image Reconstruction (STIR) [28] that modeled a GE Discovery STE PET scanner. The respiratory cycle was divided into 13 phases [see Fig. 1(b)] starting from the end-inspiration phase to the next inhalation. Three maximum respiratory diaphragm motions of 2, 3, and 4 cm were modeled in the phantoms (see Fig. 2). A spherical lesion with target-to-background ratio (TBR) of 4:1 and diameter of 25 mm was placed at the base of the right lung and close to the diaphragm, where the respiratory motion is more prominent [29]. Photon scattering and random coincidence were not modeled in this study since we were focusing on AC only.

The average of the 13 phases of the phantom activity distributions was used to generate the noise-free sinogram to simulate average of a respiratory cycle. Noisy data were then generated by adding Poisson noise based on a count level of $\sim$9.5 M, representing a 20-min whole-body PET acquisition. Three bed positions were simulated to cover the whole thoracic region in PET. For noise-free data, the CACT was represented by an average of the 13 phases of the phantom attenuation maps. The HCT, which is usually a snapshot of a respiration cycle, was generated for phase #1 (end-inspiration phase), #5 (midrespiratory phase), and #8 (end-expiration phase) of the respiration cycle, respectively, to represent the possible HCT attenuation maps (HCT-1, HCT-5, and HCT-8). For IACT, velocity matrix was obtained between the two original extreme phases, i.e., end-inspiration (phase #1) and end-expiration (phase #8) of the attenuation maps, via deformable image registration to generate the interpolated phases. The IACT was then generated by averaging the two original attenuation maps of the extreme phases, the interpolated phases and the next end-inspiration phase. Three different IACTs were simulated: 1) 2 original extreme phases + 10 interpolated phases ($\mathrm{IACT}_{2\mathrm{o}}$); 2) 2 original phases right after the end-inspiration and end-expiration phases + 10 interpolated phases ($\mathrm{IACT}_{2\mathrm{s}}$); and 3) 4 original phases (2 extreme and 2 midrespiratory phases) + 8 interpolated phases ($\mathrm{IACT}_{4\mathrm{o}}$). The $\mathrm{IACT}_{2\mathrm{s}}$ represented the slight miscapturing, i.e., "shifted version," of the two extreme phases, which might happen in the real clinical situation. For noisy CT data, CT projections were generated from different AC maps using an analytical projector and then added with Gaussian noise, which was based on the standard deviation of a region-of-interest (ROI) drawn in the liver region in the clinical CT patient data [26]. The projections were reconstructed with filtered back-projection method to get the reconstructed CT images with similar noise level as in the clinical CT data for further AC in PET.

The optical flow method (OFM), a deformable image registration algorithm based on image intensity gradient, was applied to calculate the velocity matrix that includes lateral, anterior–posterior, and inferior–superior displacement for each voxel on two successive CT phases in the respiratory cycle. This algorithm was derived based on two main assumptions: 1) the intensity of a point in the image does not change with time and 2) nearby points in the image move with a similar pattern [30], [31].

The OFM calculation is as follows [32]:

$$v_x^{(n+1)} = v_x^{(n)} - \frac{\partial f}{\partial x}\frac{\left(v_x^{(n)}\frac{\partial f}{\partial x} + v_y^{(n)}\frac{\partial f}{\partial y} + v_z^{(n)}\frac{\partial f}{\partial z} + \frac{\partial f}{\partial t}\right)}{\alpha^2 + \left(\frac{\partial f}{\partial x}\right)^2 + \left(\frac{\partial f}{\partial y}\right)^2 + \left(\frac{\partial f}{\partial z}\right)^2}$$

$$v_y^{(n+1)} = v_y^{(n)} - \frac{\partial f}{\partial y}\frac{\left(v_x^{(n)}\frac{\partial f}{\partial x} + v_y^{(n)}\frac{\partial f}{\partial y} + v_z^{(n)}\frac{\partial f}{\partial z} + \frac{\partial f}{\partial t}\right)}{\alpha^2 + \left(\frac{\partial f}{\partial x}\right)^2 + \left(\frac{\partial f}{\partial y}\right)^2 + \left(\frac{\partial f}{\partial z}\right)^2}$$

$$v_z^{(n+1)} = v_z^{(n)} - \frac{\partial f}{\partial z}\frac{\left(v_x^{(n)}\frac{\partial f}{\partial x} + v_y^{(n)}\frac{\partial f}{\partial y} + v_z^{(n)}\frac{\partial f}{\partial z} + \frac{\partial f}{\partial t}\right)}{\alpha^2 + \left(\frac{\partial f}{\partial x}\right)^2 + \left(\frac{\partial f}{\partial y}\right)^2 + \left(\frac{\partial f}{\partial z}\right)^2} \quad (1)$$

where n is the number of iterations, $v^{(n)}$ is the average velocity driven from the surrounding voxels, $f(x, y, z, t)$ is the differentiable image intensity at position (x, y, z) at time t, and α is the weighting factor with empirical value of 5. The set of recursive equations given in (1) are applied to the selected original phases of the simulated CT using a multiresolution approach to estimate the displacement field [33]. The OFM was used to generate the displacement field between the original noise-free and noisy end-inspiration and end-expiration phases, which were modeled based on a single phase of the clinical cine CT data. The total motion displacement field for each voxel in the forward motion map is equally spaced into seven intervals, leading to six sets of interpolated CT images as the midphases from inspiration to expiration. Similarly, the backward motion map is used to calculate the four midphases from expiration to inspiration [see Fig. 1(b)]. The two original, the ten interpolated phases, and the next identical end-inhalation phase compose a complete respiratory cycle. These 13 phases are averaged to generate the $\text{IACT}_{2\text{o}}$.

The noise-free and noisy PET sinograms were reconstructed using OS-EM algorithm with up to 300 updates. and ACs were conducted using noise-free and noisy HCTs, IACTs, and CACT, respectively. Their reconstructed PET images were compared based on visual assessment and analyzed in terms of the following figures of merit (FOMs):

1) *Normalized mean-square error (NMSE):* The whole reconstructed volume was used to assess the average NMSE as compared to the original phantom:

$$\text{average NMSE} = \frac{1}{m}\sum_{j=1}^{m}\left(\frac{x_j}{\overline{x}} - \frac{\lambda_j}{\overline{\lambda}}\right)^2 \quad (2)$$

where m is the number of voxels in the whole reconstructed volume, λ is the voxel count value in the original phantom, $\overline{\lambda}$ is the mean voxel value of the original phantom, x is the voxel count value in the noise-free and noisy reconstructed images, $\overline{x}$ is the mean voxel value of the reconstructed images, and j is the voxel index.

2) *Mutual information (MI):* The normalized MI $[I(X, Y)]$ between X and Y, a measure of the statistical dependence between both variables, was applied to estimate the nonlinear image intensity distribution between IACTs/HCTs/CACT and the original phantom:

$$I(X, Y) = \frac{P(X) + P(Y)}{P(X, Y)} \quad (3)$$

where X and Y are two random variables, i.e., two different images, $P(X)$ is the histogram of X, $P(Y)$ is the histogram of Y, and $P(X, Y)$ is the joint histogram of X and Y.

3) *Target-to-background ratio (TBR):* The 3-D TBR was calculated from the known lesion region and the chosen background regions in the lung in reconstructed images using different CT maps:

$$\text{TBR} = \frac{\text{Mean}_{\text{hot lesion}}}{\text{Mean}_{\text{background}}}. \quad (4)$$

4) *Contrast and noise:* We measured the average voxel value of the lesion as A_{lesion} and average voxel value in the lung as A_{lung} in the noise-free reconstructed images. The lesion contrast is defined as follows:

$$\text{Contrast} = \frac{A_{\text{lesion}} - A_{\text{lung}}}{A_{\text{lesion}} + A_{\text{lung}}}. \quad (5)$$

The noise level was measured by the normalized standard deviation (NSD) of the voxels in an approximately uniform ROI within the midlung region with a total number of 78 voxels. The NSD of the 3-D ROI was calculated by dividing the standard deviation (SD) of the ROI by the ROI mean:

$$\text{NSD} = \frac{\text{SD}}{\text{mean}} = \frac{\sqrt{\frac{1}{m-1}\sum_{j=1}^{m}(x_j - \mu)^2}}{\mu} \quad (6)$$

where m is the number of voxels in the ROI, μ is the mean voxel value of the ROI, x is the voxel count value in the noisy reconstructed images, and j is the voxel index.

5) *Image profile:* A vertical profile was drawn across the lesion and the adjacent diaphragm area to indicate the potential lesion detectability [see Fig. 3(c)].

III. Results

From visual assessment, the IACTs modeled the respiratory motions similarly to the CACT [see Fig. 3(a)]. The reconstructed PET images with AC using CACT and IACT showed no significant artifacts as compared to the original phantom (see Figs. 2(a), 3(b), and 4). Significant artifacts were observed in the PET reconstructed images using HCTs for AC in both noise-free and noisy data (see Figs. 3(d) and 4). The lesion volume and uptake was more prominent for PET reconstructed images using HCT-8 for AC, though artifacts were still observed near the diaphragm region. For $\text{IACT}_{2\text{o}}$, the lesion movement cannot be modeled exactly for motion amplitude of 4 cm, while it can be modeled for all motion amplitudes for $\text{IACT}_{4\text{o}}$ (see Fig. 5). The quantitative FOMs of NMSE and MI showed that HCT-1 and HCT-8 had the worst performances for motion amplitudes of 2 cm (see Figs. 6–8). As expected, reconstructed images using AC with CACT had least difference as compared to the original phantom, followed by $\text{IACT}_{4\text{o}}$, $\text{IACT}_{2\text{o}}$, $\text{IACT}_{2\text{s}}$, and HCT-5. Our results showed that $\text{IACT}_{2\text{o}}$ provided similar accuracy as

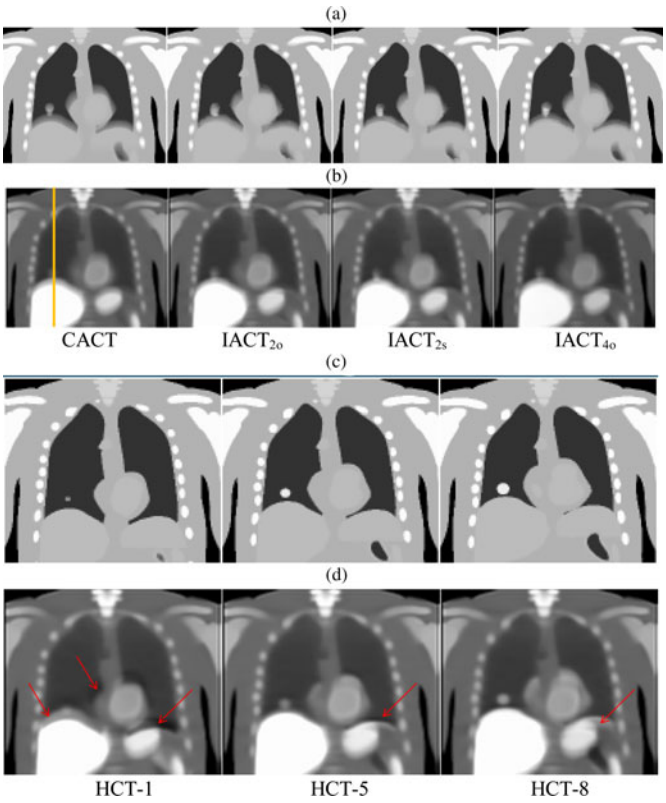

Fig. 3. (a) and (c) Different attenuation maps for AC and their corresponding PET reconstructed images [(b) and (d)] for respiratory motion = 2 cm. Significant misalignment artifacts are observed for the PET images using HCTs for AC (red arrows).

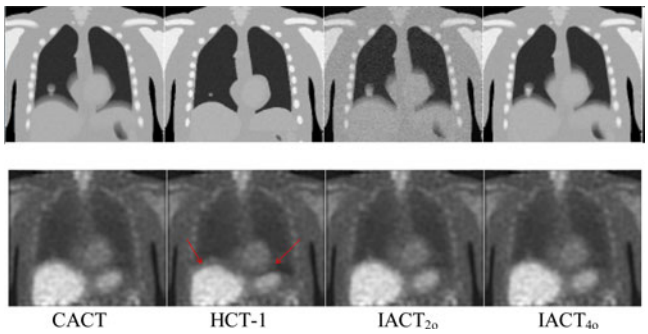

Fig. 4. (Top row) Different noisy attenuation maps for AC. (Bottom row) Their corresponding PET reconstructed images from noisy sinogram with 100 updates and Butterworth filtering with cutoff frequency of 0.21 pixel^{-1} for maximum respiratory motion of 2 cm. Significant misalignment artifacts are observed for the PET images using HCTs for AC (red arrows).

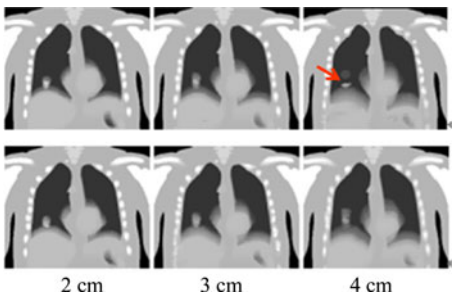

Fig. 5. (Top row) IACT$_{2o}$ and (bottom row) IACT$_{4o}$ maps for three different motion amplitudes. The lesion movement cannot be modeled exactly for IACT$_{2o}$ in motion = 4 cm (red arrow).

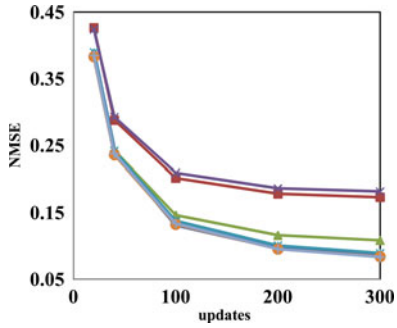

Fig. 6. Noise-free results of NMSE for respiratory motion of 2 cm.

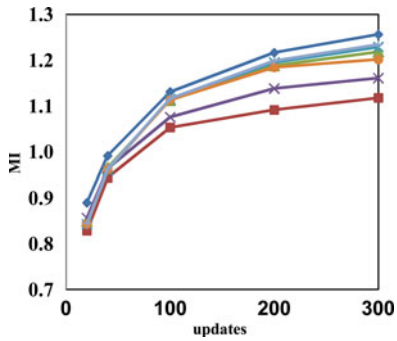

Fig. 7. Noise-free results of MI for respiratory motion of 2 cm.

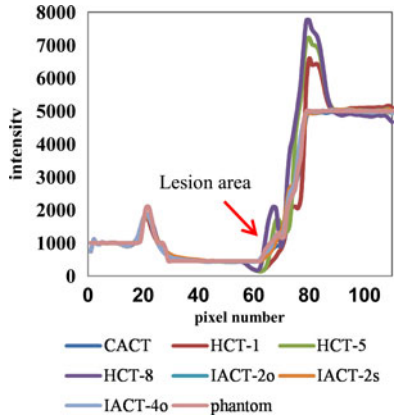

Fig. 8. Noise-free results of image profiles for respiratory motion of 2 cm.

compared to IACT$_{4o}$ and even CACT, with MI difference of <0.41% and <2.17%, respectively, thereby reassuring our findings in the previous clinical studies. With a slight misplacement of these two phases, the resultant IACT$_{2s}$ still showed comparable accuracy to IACT$_{2o}$ with MI difference of <2.23%. Noise-free (see Figs. 6 and 7) and noisy simulations (see Figs. 9 and 10) had accordant results, no matter the noisy IACTs were obtained from noise-free or noisy phases. For the TBR results, AC with HCT-1 showed inferior results as compared to others (see Fig. 11), as also indicated by visual assessment [see Fig. 3(d)]. IACTs performed similarly as compared to CACT for AC in terms of TBR (see Fig. 11), while HCT-8 showed higher TBR as compared to others. Image profiles results are also accordant with visual assessment that HCT-8 and HCT-5

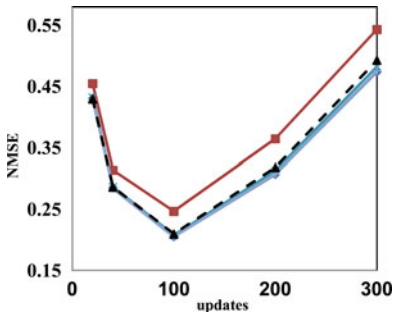

Fig. 9. Noisy results of NMSE for respiratory motion of 2 cm. Dotted lines (IACT-2o_noise) are the results for noisy $IACT_{2o}$ that are generated from two noisy single CT phases.

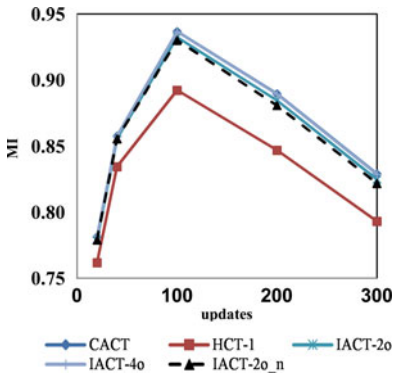

Fig. 10. Noisy results of MI for respiratory motion of 2 cm. Dotted lines (IACT-2o_noise) are the results for noisy $IACT_{2o}$ that are generated from two noisy single CT phases.

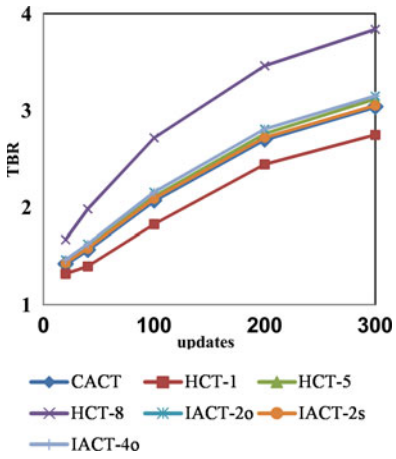

Fig. 11. Noise-free results of TBR for respiratory motion of 2 cm.

provide better lesion detectability as compared to others but they caused artifactual increase of diaphragmatic uptake near the liver (see Fig. 8). Fig. 12 shows the relationship between lesion contrast and NSD for different AC schemes. The points on the curves represented number of updates, increasing from the left to the right side for OS-EM algorithm. The bottom-right region indicated better image quality, i.e., lower noise and higher contrast. The HCT-1 clearly showed inferior noise–

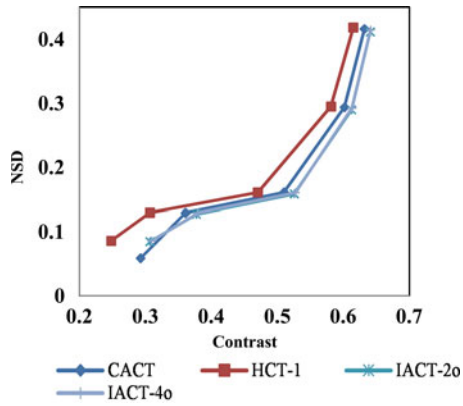

Fig. 12. Image noise level as a function of lesion contrast for different AC schemes for respiratory motion of 2 cm.

contrast tradeoff among the four curves. A summary of the noise-free results for motion amplitude of 2, 3, and 4 cm of 300 updates is given in Table I.

IV. Discussion

One limitation for our study is that the HCTs we simulated using XCAT phantom represented a snapshot of free-breathing state, i.e., the CT acquired when the patients did not take any breath-hold. Thus, one can infer that the improvement of IACT as compared to realistic breath-hold HCT would be more significant. However, the use of the free-breathing extreme phases was suitable for generating IACT in this simulation study. For the global measurement of image quality such as NMSE and MI (see Figs. 6 and 7; see Table I), HCT-5 showed the best performance among HCTs in this study. It matched with our predictions that mid-phase HCT is probably more similar to CACT as compared to breath-hold CTs, i.e., HCT-1 and HCT-8. However, HCT-5 still worked slightly inferior to the IACTs quantitatively. Also, it is clinically difficult to assure that the HCT-5, i.e., midphase of the respiratory cycle, would be captured for the HCT acquisition, as it is difficult for patients to hold their breath during the midrespiratory phases. The NMSE and MI results were generally in accordance. On the other hand, for the FOM more related to lesion detection such as TBR and image profile, HCT-8/HCT-5 showed even better performance as compared to CACT for AC (see Figs. 11 and 8), probably due to the fact that HCT-8 coincidently captured the lesion with its full size in this case. The advantage of HCT-8 for AC may cease for lesions located at other regions of the thorax, as indicated by the NMSE and MI results. Moreover, noise–contrast tradeoff has been validated to correlate well with task-based observer study [34], and HCT-1 showed the worst lesion detectability in all detection-related FOMs, matched with the visual assessment that the diaphragm mismatch artifacts blurred out the lesion and caused the uptake underestimation. Different breathing patterns for CT acquisition in PET/CT were investigated, including normal-expiration breath-hold [35], [36], i.e., similar to HCT-8 in this study, and deep-inspiration breath-hold (DIBH) PET/CT [37], [38].

TABLE I
SUMMARY OF THE NOISE-FREE RESULTS OF DIFFERENT CT AC METHODS AT 300 UPDATES

Motion amplitude	FOM	CACT	HCT-1	HCT-5	HCT-8	$IACT_{2o}$	$IACT_{2s}$	$IACT_{4o}$
2 cm	NMSE	0.085	0.140	0.094	0.139	0.088	0.086	0.093
	MI	1.256	1.118	1.218	1.161	1.229	1.234	1.201
	TBR	3.040	2.748	3.118	3.838	3.149	3.149	3.051
3 cm	NMSE	0.084	0.173	0.108	0.182	0.089	0.083	0.084
	MI	1.218	1.036	1.160	1.086	1.176	1.210	1.193
	TBR	2.477	2.427	2.410	3.439	2.622	2.513	2.495
4 cm	NMSE	0.078	0.204	0.120	0.222	0.090	0.082	0.089
	MI	1.324	1.085	1.228	1.153	1.247	1.303	1.241
	TBR	2.089	2.094	1.955	2.988	1.851	2.055	1.708

In order to reduce data redundancy, we just simulated the noise based on the clinical data for CACT, HCT-1, $IACT_{2o}$, and $IACT_{4o}$ [see Figs. 4, 9, 10, and 12], as HCT-5 and HCT-8 should have the similar noise level as compared to HCT-1 and $IACT_{2s}$ should have the similar noise level as compared to $IACT_{2o}$ in the noisy CT simulations. The noisy simulation results for a motion of 3 cm were in accordance with those of the motion of 2 cm and were not shown here. Generating IACTs using noisy CT phases was a more realistic representation for the clinical data with higher noise and lower radiation dose. However, we compared the noisy IACTs generated by noisy respiratory phases (IACT-2o_noise) and noise-free phases (IACT-2o), i.e., noise directly modeled on the resultant IACT based on the clinical IACT data. Their results were similar, indicating that the noise level on the realistic single CT phase did not significantly affect the OFM calculation in this study (see Figs. 9 and 10). Our preliminary study applying the IACT on real clinical patients also demonstrated improved AC results with $\sim$87% dose reduction while using the realistic noisy phases for motion modeling and interpolation [41].

Our results showed that IACT method using four original phases ($IACT_{4o}$) worked well for maximum breathing motion amplitude of 4 cm. Although the IACT method using two original phases ($IACT_{2o}$) did not model the lesion movement of 4 cm in this particular phantom (see Fig. 5), the global quantitative FOMs still showed similar image quality improvement of IACT as compared to HCTs for motion amplitudes of 2, 3, and 4 cm (see Table I). A clinical study with $\sim$100 patients showed that $\sim$90% of the clinical patients had $\leq$3 cm respiratory motion amplitude and $\sim$95% of patients had $\leq$4 cm motion [19], indicating that the IACT method should work well for most of the patients. Besides, slight time errors may exist for capturing these two extreme phases in the real clinical situations. However, our results of $IACT_{2s}$, i.e., with "shifted" end-inspiration and end-expiration phases for interpolation, were very similar to $IACT_{2o}$, indicating the robustness of this method. Our previous work suggested that using the average of two extreme phases for AC generally showed inferior performance as compared to the IACT methods, probably attributed to the improved respiratory motion modeling using the OFM approach [26]. Generating the IACT using just the end-expiration and end-inspiration phases would have the minimal dose. It may also be feasible to achieve the same dose reduction of using only two original phases for interpolation with improved image quality by using more phases for interpolation and reducing the dose for each phase at the same time, as our current study hints that $IACT_{4o}$ works well for larger motion amplitude and more closely mimics CACT. However, capturing multiple phases during a respiratory cycle may not be feasible in clinical practice with the considerations of X-ray beam ON/OFF delay.

Hamill *et al*. [39] showed that smaller lesions were more affected by the respiratory motion blurring, i.e., quantitation of 20 mm tumors was still feasible for conventional PET/CT protocol when the motion is less than 15 mm, while 10 mm tumors were more significantly blurred and their SUV values were more underestimated than those of the 20 mm tumors. Tumors with 30 mm diameter were blurred less. Pevsner *et al.* [4] showed that the underestimation of the activity concentration in the sphere phantoms can reach 75% for the standard clinical protocol, depending on the spherical sizes. Our results showed that the IACT method works for a 25 mm lesion for motion amplitude of $\sim$3 cm. We are currently investigating the effects of lesion sizes, lesion uptake ratios and lesion locations on the proposed methods and preliminary results showed that smaller lesions with lower TBR would be more challenging to model for IACT.

The two extreme phases used for IACT cannot be obtained via patients' voluntary breath-holding, as they would be very different from the free-breathing state as in the PET and would generate respiratory artifacts. Thus, the clinical realization of the IACT technique highly relies on the implementation of the active breathing control (ABC) device to ensure the captured respiratory phases represent a free-breathing state of the patients [40]. An associated hardware and acquisition software has been developed for a preliminary PET/CT study on patients [41].

V. CONCLUSION

In this study, we have evaluated and analyzed the effectiveness of IACT as compared to CACT and HCT using simulations with ground truth. We concluded that IACT is a robust, accurate low-dose alternate to CACT and works well for a large range of respiratory motion amplitudes. Further, optimization of IACT protocol with the consideration of dose reduction and actual clinical implementation of IACT using ABC are warranted.

ACKNOWLEDGMENT

The authors would like to thank Dr. J. Xu and Dr. Y. Du from the Division of Medical Imaging Physics, Department of Radiology, Johns Hopkins University, for their suggestions on CT noise modeling and helpful discussions in preparing the manuscript. The authors would also like to thank M.-B. Chang from the Graduate Institute of Clinical Medical Science, China Medical University, for her assistance in data analysis and P. A. Mou from the Department of Electrical and Computer Engineering, University of Macau, for IT support.

REFERENCES

[1] R. de Juan, B. Seifert, T. Berthold, G. K. von Schulthess, and G. W. Goerres, "Clinical evaluation of a breathing protocol for PET/CT," *Eur. Radiol.*, vol. 14, pp. 1118–1123, 2004.

[2] K. L. Gould, T. Pan, C. Loghin, N. P. Johnson, A. Guha, and S. Sdringola, "Frequent diagnostic errors in cardiac PET/CT due to misregistration of CT attenuation and emission PET images: A definitive analysis of causes, consequences, and corrections," *J. Nucl. Med.*, vol. 48, pp. 1112–1121, 2007.

[3] Y. E. Erdi, S. A. Nehmeh, T. Pan, A. Pevsner, K. E. Rosenzweig, G. Mageras, E. D. Yorke, H. Schoder, W. Hsiao, O. D. Squire, P. Vernon, J. B. Ashman, H. Mostafavi, S. M. Larson, and J. L. Humm, "The CT motion quantitation of lung lesions and its impact on PET-measured SUVs," *J. Nucl. Med.*, vol. 45, pp. 1287–1292, 2004.

[4] A. Pevsner, S. A. Nehmeh, J. L. Humm, G. S. Mageras, and Y. E. Erdi, "Effect of motion on tracer activity determination in CT attenuation corrected PET images: A lung phantom study," *Med. Phys.*, vol. 32, pp. 2358–2362, 2005.

[5] G. Cook, E. Wegner, and I. Fogelman, "Pitfalls and artifacts in FDG PET and PET/CT oncologic imaging," *Semin. Nucl. Med.*, vol. 34, pp. 122–133, 2004.

[6] M. M. Osman, C. Cohade, Y. Nakamoto, L. T. Marshall, J. P. Leal, and R. L. Wahl, "Clinically significant inaccurate localization of lesions with PET/CT: Frequency in 300 patients," *J. Nucl. Med.*, vol. 44, pp. 240–243, 2003.

[7] L. Boucher, S. Rodrigue, R. Lecomte, and F. Benard, "Respiratory gating for 3-dimensional PET of the thorax: Feasibility and initial results," *J. Nucl. Med.*, vol. 45, pp. 214–219, Feb. 2004.

[8] F. Ponisch, C. Richter, U. Just, and W. Enghardt, "Attenuation correction of four dimensional (4D) PET using phase-correlated 4D-computed tomography," *Phys. Med. Biol.*, vol. 53, pp. N259–N268, Jul. 7, 2008.

[9] S. A. Nehmeh, Y. E. Erdi, T. Pan, A. Pevsner, K. E. Rosenzweig, E. Yorke, G. S. Mageras, H. Schoder, P. Vernon, O. Squire, H. Mostafavi, S. M. Larson, and J. L. Humm, "Four-dimensional (4D) PET/CT imaging of the thorax," *Med. Phys.*, vol. 31, pp. 3179–3186, Dec. 2004.

[10] S. J. McQuaid, T. Lambrou, and B. F. Hutton, "A novel method for incorporating respiratory-matched attenuation correction in the motion correction of cardiac PET-CT studies," *Phys. Med. Biol.*, vol. 56, pp. 2903–2915, May 2011.

[11] R. G. Wells, T. D. Ruddy, R. A. DeKemp, J. N. DaSilva, and R. S. Beanlands, "Single-phase CT aligned to gated PET for respiratory motion correction in cardiac PET/CT," *J. Nucl. Med.*, vol. 51, pp. 1182–1190, Aug. 2010.

[12] C. Liu, A. Alessio, L. Pierce, K. Thielemans, S. Wollenweber, A. Ganin, and P. Kinahan, "Quiescent period respiratory gating for PET/CT," *Med. Phys.*, vol. 37, pp. 5037–5043, Sept. 2010.

[13] T. F. Li, B. Thorndyke, E. Schreibmann, Y. Yang, and L. Xing, "Model-based image reconstruction for four-dimensional PET," *Med. Phys.*, vol. 33, pp. 1288–1298, May 2006.

[14] F. Qiao, T. Pan, J. W. Clark, and O. R. Mawlawi, "A motion-incorporated reconstruction method for gated PET studies," *Phys. Med. Biol.*, vol. 51, pp. 3769–3783, Aug. 2006.

[15] F. Lamare, M. J. L. Carbayo, T. Cresson, G. Kontaxakis, A. Santos, C. C. Le Rest, A. J. Reader, and D. Visvikis, "List-mode-based reconstruction for respiratory motion correction in PET using non-rigid body transformations," *Phys. Med. Biol.*, vol. 52, pp. 5187–5204, Sept. 2007.

[16] N. Grotus, A. J. Reader, S. Stute, J. C. Rosenwald, P. Giraud, and I. Buvat, "Fully 4D list-mode reconstruction applied to respiratory-gated PET scans," *Phys. Med. Biol.*, vol. 54, pp. 1705–1721, Mar. 2009.

[17] F. J. Lagerwaard, J. R. V. de Koste, M. R. J. Nijssen-Visser, R. H. Schuchhard-Schipper, S. S. Oei, A. Munne, and S. Senan, "Multiple "slow" CT scans for incorporating lung tumor mobility in radiotherapy planning," *Int. J. Radiat. Oncol.*, vol. 51, pp. 932–937, Nov. 2001.

[18] J. A. Nye, F. Esteves, and J. R. Votaw, "Minimizing artifacts resulting from respiratory and cardiac motion by optimization of the transmission scan in cardiac PET/CT," *Med. Phys.*, vol. 34, pp. 1901–1906, Jun. 2007.

[19] T. S. Pan, O. Mawlawi, S. A. Nehmeh, Y. E. Erdi, D. S. Luo, H. H. Liu, R. Castillo, R. Mohan, Z. X. Liao, and H. A. Macapinlac, "Attenuation correction of PET images with respiration-averaged CT images in PET/CT," *J. Nucl. Med.*, vol. 46, pp. 1481–1487, 2005.

[20] R. A. H. Cook, G. Carnes, T. Y. Lee, and R. G. Wells, "Respiration-averaged CT for attenuation correction in canine cardiac PET/CT," *J. Nucl. Med.*, vol. 48, pp. 811–818, 2007.

[21] A. M. Alessio, S. Kohlmyer, K. Branch, G. Chen, J. Caldwell, and P. Kinahan, "Cine CT for attenuation correction in cardiac PET/CT," *J. Nucl. Med.*, vol. 48, pp. 794–801, 2007.

[22] E. Kamel, T. F. Hany, C. Burger, V. Treyer, A. H. R. Lonn, G. K. von Schulthess, and A. Buck, "CT vs Ge-68 attenuation correction in a combined PET/CT system: evaluation of the effect of lowering the CT tube current," *Eur. J. Nucl. Med. Mol. Imaging*, vol. 29, pp. 346–350, 2002.

[23] T. Xia, A. M. Alessio, B. D. Man, R. Manjeshwar, E. Asma, and P. E. Kinahan, "Ultra-low dose CT attenuation correction for PET/CT," *Phys. Med. Biol.*, vol. 57, pp. 309–328, 2012.

[24] K. L. Gould, T. Pan, C. Loghin, N. P. Johnson, and S. Sdringola, "Reducing radiation dose in rest-stress cardiac PET/CT by single poststress cine CT for attenuation correction: Quantitative validation," *J. Nucl. Med.*, vol. 49, pp. 738–745, 2008.

[25] T. Sun and G. S. P. Mok, "Techniques for respiration-induced artifacts reductions in thoracic PET/CT," *Quant. Imaging. Med. Surg.*, vol. 2, pp. 46–52, 2012.

[26] T. C. Huang, G. S. P. Mok, S. J. Wang, T. H. Wu, and G. Zhang, "Attenuation correction of PET images with interpolated average CT for thoracic tumors," *Phys. Med. Biol.*, vol. 56, pp. 2559–2567, 2011.

[27] T. H. Wu, G. Zhang, S. J. Wang, C. H. Chen, B. H. Yang, N. Y. Wu, and T. C. Huang, "Low-dose interpolated average CT for attenuation correction in cardiac PET/CT," *Nucl. Instrum. Methods Phys. Res. A*, vol. 619, pp. 361–364, 2010.

[28] K. Thielemans, C. Tsoumpas, S. Mustafovic, T. Beisel, P. Aguiar, N. Dikaios, and M. W. Jacobson, "STIR: Software for Tomographic Image Reconstruction Release 2," *Phys. Med. Biol.*, vol. 57, pp. 867–883, 2012.

[29] E. Tonkopi, P. C. M. Chi, O. Mawlawi, A. C. Riegel, E. M. Rohren, H. A. Macapinlac, and T. Pan, "Average CT in PET studies of colorectal cancer patients with metastasis in the liver and esophageal cancer patients," *J. Appl. Clin. Med. Phys.*, vol. 11, pp. 217–228, 2010.

[30] T. C. Huang, G. Zhang, T. Guerrero, G. Starkschall, K. P. Lin, and K. Forster, "Semi-automated CT segmentation using optic flow and Fourier interpolation techniques," *Comput. Methods Prog. Bio.*, vol. 84, pp. 124–134, 2006.

[31] B. K. P. Horn and B. G. Schunck, "Determining optical-flow," *Artif. Intell.*, vol. 17, pp. 185–203, 1981.

[32] G. Zhang, T. C. Huang, T. Guerrero, K. P. Lin, C. Stevens, G. Starkschall, and K. Forster, "Use of three-dimensional (3D) optical flow method in mapping 3D anatomic structure and tumor contours across four-dimensional computed tomography data," *J. Appl. Clin. Med. Phys.*, vol. 9, pp. 59–69, 2008.

[33] G. G. Zhang, T. C. Huang, K. M. Forster, K. P. Lin, C. Stevens, E. Harris, and T. Guerrero, "Dose mapping: Validation in 4D dosimetry with measurements and application in radiotherapy follow-up evaluation," *Comput. Methods Prog. Biol.*, vol. 90, pp. 25–37, 2008.

[34] C. Liu, J. Y. Xu, and B. M. W. Tsui, "Myocardial perfusion SPECT using a rotating multi-segment slant-hole collimator," *Med. Phys.*, vol. 37, pp. 1610–1618, Apr. 2010.

[35] G. W. Goerres, E. Kamel, B. Seifert, C. Burger, A. Buck, T. F. Hany, and G. K. von Schulthess, "Accuracy of image coregistration of pulmonary lesions in patients with non-small cell lung cancer using an integrated PET/CT system," *J. Nucl. Med.*, vol. 43, pp. 1469–1475, 2002.

[36] G. W. Goerres, E. Kamel, T. N. H. Heidelberg, M. R. Schwitter, C. Burger, and G. K. von Schulthess, "PET-CT image co-registration in the thorax: influence of respiration," *Eur. J. Nucl. Med. Mol. Imaging*, vol. 29, pp. 351–360, 2002.

[37] G. S. Meirelles, Y. E. Erdi, S. A. Nehmeh, O. D. Squire, S. M. Larson, J. L. Humm, and H. Schoder, "Deep-inspiration breath-hold PET/CT:

Clinical findings with a new technique for detection and characterization of thoracic lesions," *J. Nucl. Med.*, vol. 48, pp. 712–719, 2007.

[38] S. A. Nehmeh, Y. E. Erdi, G. S. P. Meirelles, O. Squire, S. M. Larson, J. L. Humm, and H. Schoder, "Deep-inspiration breath-hold PET/CT of the thorax," *J. Nucl. Med.*, vol. 48, pp. 22–26, Jan. 2007.

[39] J. J. Hamill, G. Bosmans, and A. Dekker, "Respiratory-gated CT as a tool for the simulation of breathing artifacts in PET and PET/CT," *Med. Phys.*, vol. 35, pp. 576–585, Feb. 2008.

[40] J. W. Wong, M. B. Sharpe, D. A. Jaffray, V. R. Kini, J. M. Robertson, J. S. Stromberg, and A. A. Martinez, "The use of active breathing control (ABC) to reduce margin for breathing motion," *Int. J. Radiat. Oncol.*, vol. 44, pp. 911–919, 1999.

[41] T. Sun, T. H. Wu, N. Y. Wu, and G. S. P. Mok, "Low dose interpolated average CT for PET/CT attenuation correction using an active breathing controller (ABC)," in *Proc. IEEE Nucl. Sci. Symp. Med. Imag. Conf. Rec.*. Anaheim, CA, USA, 2012, pp. 2856–2858.

Authors' photographs and biographies not available at the time of publication.